Journal of Volcanology and Geothermal Research 410 (2021) 107144

Contents lists available at ScienceDirect

Journal of Volcanology and Geothermal Research

journal homepage: www.elsevier.com/locate/jvolgeores

Invited Research Article

The volatile budget of Hawaiian magmatism: Constraints from melt inclusions from Haleakala volcano, Hawaii

L.R. Moore [a,*], E. Gazel [b], R.J. Bodnar [a]

[a] Department of Geosciences, Virginia Tech, Blacksburg, VA 24061, USA
[b] Department of Earth and Atmospheric Sciences, Cornell University, Ithaca, NY 14853-1504, USA

ARTICLE INFO

Article history:
Received 1 September 2020
Received in revised form 23 November 2020
Accepted 24 November 2020
Available online 5 December 2020

Keywords:
Hawaii
Post-shield stage
Melt inclusion
CO_2
Volatiles

ABSTRACT

Pre-eruptive volatile contents recorded by melt inclusions from ocean island settings such as Hawaii constrain the extent of deep Earth outgassing on geologic timescales by mantle plume activity. However, melt inclusions trapped from a partially degassed magma will not reflect the original volatile content of the primary melt, and relatively silicic (>45 wt% SiO_2) shield-stage tholeiites are more likely to have been affected by degassing during fractionation at shallow depths. In contrast, magmas associated with post-shield volcanoes erupt volatile-rich melts that ascend quickly from the source region and crystallize in deep reservoirs. As a result, melt inclusions from post-shield volcanoes may be more likely to preserve undegassed melt compositions that can be used to determine the primary melt and source volatile contents. In this study, we analyzed melt inclusions from Haleakala Volcano (East Maui, Hawaii) to estimate the volatile budget of Hawaiian post-shield magmas. Melt inclusions from Haleakala contain up to 1.3 wt% CO_2, 1.2 wt% H_2O, and about 2000 ppm S. We calculate that melts from Haleakala were derived from a parental melt with ~0.7 wt% H_2O and ~0.7 wt% CO_2 and experienced ~15–40% polybaric, fluid-saturated crystallization starting at 5–7 kbar. Post-shield melt inclusions from Haleakala have H_2O/Ce and CO_2/Ba compositions that are intermediate between shield-stage melt inclusions from Kilauea and the alkaline North Arch Volcanic Field, which is consistent with a scenario in which primary melts from Haleakala are influenced by the volatile-rich auto-metasomatized periphery of the composite plume source.

1. Introduction

1.1. Mantle plumes and Hawaiian magmatism

Mantle plumes are thought to transfer volatiles from the deep Earth to the surface, and thus represent an important mechanism of planetary outgassing (Dasgupta and Hirschmann, 2010; Dasgupta et al., 2013). Many oceanic island volcanoes are situated above mantle plumes which are inferred to rise from the deep lower mantle to the base of the lithosphere to feed hot-spot melting (French and Romanowicz, 2015), and the compositions of the related ocean island basalts (OIBs) have been used to assess the composition of deep mantle materials (Hofmann and White, 1982; Hofmann, 2003). Additionally, alkaline basalts from OIB settings may be derived from partial melting of a CO_2-rich, ultramafic mantle source (Edgar, 1987; Hémond et al., 1994; Dasgupta et al., 2007). Therefore, understanding the nature of plume melting and volcanism – especially alkaline volcanism from OIBs – is crucial to understanding planetary degassing.

Hawaii is perhaps the best-characterized volcanic setting on the planet and is a natural laboratory for studying plume melting. As the Pacific plate moves across the hot spot below Hawaii, the islands that form evolve through a progression of volcanic stages which are characterized by changes in eruptive volume, eruptive style, and melt composition (Peterson and Moore, 1987). Island growth begins with a "pre-shield" seamount stage, which is characterized by a relatively low volume of alkaline melt. This is followed by a voluminous "shield stage" during which most of the volume of the island is generated by the eruption of tholeiitic lava. The output volume of the volcano progressively decreases with time, and erupted material becomes more alkaline as the island transitions into a "post-shield" or "capping" stage as deeper and more ephemeral magma chambers develop (Frey et al., 1990). Volcanic activity may cease entirely after this stage, and the volume of the island decreases with time because material removed by erosion is not replenished by new volcanic material. Intermittent volcanic activity may continue during or after this erosion-dominated period, and islands that have experienced low-volume eruptions of highly alkaline, silica-undersaturated lava after a significant amount of erosion has occurred are said to be in the "rejuvenated" or "post-erosional" stage (Clague and Dalrymple, 1987). Subaerial rejuvenated volcanism is similar in composition to explosive, highly alkaline submarine volcanic deposits

* Corresponding author at: 4044 Derring Hall, Virginia Tech, 926 West Campus Drive, Blacksburg, VA 24061, USA.
E-mail address: moorelr@vt.edu (L.R. Moore).

https://doi.org/10.1016/j.jvolgeores.2020.107144
0377-0273/

which are present in a positive topographic anomaly located near O'ahu and Kaua'I, approximately 500 km from the plume center. Arguably the most well-characterized of these localities is the North Arch Volcanic Field (e.g. Frey et al., 2000; Dixon et al., 1997) located ~200 km north of Oahu.

In addition to geochemical and petrologic variation in volcanic behavior, the Hawaiian plume is also isotopically heterogeneous over space and time. Volcanic edifices are isotopically diverse (Tatsumoto, 1978) and may be divided into two parallel groups along the island chain based on their Pb isotopic compositions (KEA and LOA endmember compositions; Abouchami et al., 2005). In addition to the LOA and KEA endmember compositions shared by shield-stage melts, rejuvenated and post-shield stage melts also contain a proportion of an isotopically-depleted endmember component (e.g. Bizimis et al., 2013; Phillips et al., 2016), which increases with time based on stratigraphic position and with distance from the hot spot (Garcia et al., 2010; Clague and Sherrod, 2014). Models invoked to explain isotopic variations have had features that include 1) progressive incorporation of external oceanic material into the plume with time (e.g. Frey et al., 1990), 2) randomly- or laterally-distributed regions of isotopically distinct material within the plume (e.g. Ito and Mahoney, 2005; Hofmann and Farnetani, 2013) which are preferentially sampled depending on the degree of melting (e.g. Garcia et al., 2010), 3) orientation of the plume relative to plate motion (Jones et al., 2017), and 4) temporal variations related to internal mixing within the plume (Ballmer et al., 2013). These proposed scenarios have evolved over recent decades to accommodate an increasing number of geologic, geochemical, and geophysical observations.

While the combined volcano-stage model and geodynamic plume models together provide a robust framework which can explain the geologic and geochemical properties of the Hawaiian islands, the transitions between each stage of growth and their causes are not as well understood. The gradual changes in melt composition between the pre-shield, shield, and post-shield stages can be explained by variable degrees of melting as a function of distance from the hot spot (Liu and Chase, 1991). In contrast, explaining the eruptive hiatus from the post-shield stage to the rejuvenated stage requires additional processes such as crustal flexure (Bianco et al., 2005) and/or secondary melting of mantle source material (Ribe and Christensen, 1999). However, the transitions between the stages of volcanic activity can be gradual rather than punctuated (Clague and Sherrod, 2014), and inferred changes in melt supply may also be accompanied by changes in source composition – even within the same volcanic edifice (Chen et al., 1991; Blichert-Toft et al., 2003; Xu et al., 2005; Garcia et al., 2010).

Geodynamic modeling has suggested that differences in both eruptive behavior and isotopic heterogeneity are related to compositional variation within the plume, which can give rise to complex upwelling behavior and variable melt output (Ballmer et al., 2013) due to the presence of a recycled eclogite component within the plume (Hofmann and Jochum, 1996; Hauri, 1996). This recycled eclogite component is thought to begin melting deeper than ~150 km (Sobolev et al., 2005) and contribute to concentric chemical zonation of the plume observed in the geographic distribution of trace element enrichment of erupted melts (Dixon and Clague, 2001). In particular, it is thought that the outer portion of the Hawaiian plume is enriched in volatiles as a result of auto-metasomatism by fluids derived from deep eclogite melting within the Hawaiian plume (Dixon and Clague, 2001; Dixon et al., 2008), and this zonation should be reflected in the volatile budgets of magmas crystallizing at different distances from the center of the plume.

Constraining the volatile budget of melts from the Hawaiian plume is challenging owing to the strong pressure dependence of volatile solubility in silicate melts, which controls the depth at which degassing begins within the volcanic "plumbing system" (e.g. Dixon and Clague, 2001). Submarine lavas provide a crucial source of petrologic information about the pre-eruptive volatile content of the melt and mantle source owing to limited degassing at hydrostatic pressure. This is in contrast to subsequent, more enhanced open-system degassing which occurs when volcanoes breach the water surface (e.g. Moore, 1965). For example, analyses of submarine samples collected at Puna Ridge indicate that early mixing of previously degassed and more volatile-rich undegassed melts exert an early control on the volatile content of primitive magmas (Dixon et al., 1991). As the pre-eruptive volatile content of the magma is increased by crystallization, the volatile content of the source can be estimated from analyses of picritic glasses by modeling the process of olivine crystallization (e.g. Clague et al., 1991). Additionally, based partly on 1) the propensity for strongly alkaline melts to experience minimal degassing compared to tholeiitic magmas (e.g. Dixon, 1997) and 2) the significant hydrostatic pressure (~400 bar) at the site of eruption, the North Arch Volcanic Field (NAVF) was investigated to explore the phenomenon of volcanism at the periphery of the plume where alkaline lavas were found erupting in equilibrium with a CO_2-rich exsolved fluid (Dixon et al., 1997). Data collected from submarine samples distributed across the plume have informed a family of melting models that involve a variably mixed composite of the volatile-poor Hawaiian plume core, a relatively volatile-rich "sheath," and metasomatizing silicic and carbonatitic fluids (Dixon et al., 2008). This inferred auto-metasomatism on the periphery of the plume is inferred to be expressed isotopically as the KOO (Koolau) endmember component in contrast to the relatively dry plume component inferred to be associated with Loihi at the center of the plume (Dixon and Clague, 2001).

1.2. Melt inclusions and degassing

A complementary approach to the analysis of submarine and subaerial lava samples is to analyze melt inclusions trapped in minerals that crystallized at depth, which ideally have trapped a sample of melt that had experienced minimal degassing, and which have remained closed from the ambient environment. In general, mineral crystallization depths are inferred to occur at greater pressures than those present on the seafloor (e.g. Hammer et al., 2016). Previous inferences of the relatively dry composition of the Hawaiian plume core were made by comparing bulk analyses of olivine-hosted melt inclusions (Delaney et al., 1978) to analyses of glassy rinds on dredged pillow basalts (e.g. Moore, 1970). In cases where melt inclusions are trapped during degassing at fluid-saturated conditions, the volatile contents of melt inclusions can be used to determine the pressure at the time of crystallization using an experimentally defined volatile-melt solubility relationship (Metrich and Wallace, 2008). Using this approach, individual microanalyses of melt inclusions in olivine phenocrysts from Kilauea have improved the general understanding that the observed volatile content of shield-stage magmas is dominated by shallow degassing and mixing processes (e.g. Dixon et al., 1991; Anderson and Brown, 1993) where re-mixing of degassed magma by drainback can deplete the bulk volatile contents of basaltic magmas in shallow storage reservoirs at Kilauea – both in the summit region and along the rift zones (Wallace and Anderson, 1998).

While melt inclusions have been used to estimate the pre-eruptive volatile contents of shield and post-shield stage melts from Hawaii (e.g. Wallace and Anderson, 1998; Sobolev et al., 2011; Sides et al., 2014; Tucker et al., 2019), obtaining accurate volatile contents is challenging because of CO_2 lost to bubbles which form in the inclusion after trapping (Roedder, 1979; Anderson and Brown, 1993; Steele-MacInnis et al., 2011; Moore et al., 2015). Tucker et al. (2019) recently reported analyses of melt inclusions from several Hawaiian volcanoes with CO_2 contents determined using an equation of state to estimate the amount of CO_2 contained in the bubble. In this study, we use Raman spectroscopy to measure the CO_2 content of melt inclusion bubbles *in situ* as has been done in several recent studies (e.g. Esposito et al., 2011; Hartley et al., 2014; Moore et al., 2015; Aster et al., 2016). This approach has the advantage of avoiding uncertainties associated with nonequilibrium volume exsolution related to contraction of the bubble during eruption as discussed by Wallace et al. (2015) and Moore et al. (2015, 2018). This Raman approach also has the disadvantage that the

observed density of CO_2 in the vapor bubble may have been modified by subsolidus reactions between the fluid in the bubble and the surrounding glass to produce carbonate phases, as has been observed in other MI studies (c.f., Esposito et al., 2016). Further details are discussed below and in supplementary material.

To explore the relationship between the volatile budget of Hawaiian volcanoes at different growth stages, we used melt inclusions from Haleakala Volcano to estimate the source volatile content and melt degassing behavior during crystallization. Haleakala is a ~2 million-year old volcanic complex on East Maui that has experienced all of the stages of volcanic growth through the end of the post-shield stage (Sherrod et al., 2003, 2007). The most recent volcanism at Haleakala (~1 Ma to present) consists of monogenetic volcanic vents that cut across a deeply incised erosional surface. However, detailed stratigraphic age dating indicates that Haleakala has yet to experience an eruptive hiatus that is indicative of the transition from post-shield to rejuvenated volcanism, but can be considered to be approaching the end of its post-shield stage based on 1) the duration of post-shield volcanism present on other Hawaiian islands and 2) discrete lapses in volcanic activity evident in the stratigraphic record (Sherrod et al., 2003). Additionally, isotopic compositions of melts from Haleakala's Hana and Kula post-shield volcanism suggest a mixed composition between a KEA-like composition and a depleted composition (Phillips et al., 2016). Haleakala therefore represents the oldest and most distal site of post-shield volcanism on Hawaii with respect to the center of the plume, with a composition influenced by an isotopically-defined depleted rejuvenated mantle endmember component (DRC; e.g. after Bizimis et al., 2013) which also provides opportunities to sample melt inclusions from fresh, monogenetic cinder cones. This is important because rapidly-quenched melt inclusions are less likely to have experienced significant post-entrapment crystallization (Roedder, 1979; Bodnar and Student, 2006; Steele-MacInnis et al., 2011) and H_2O loss (Danyushevsky et al., 2002; Lloyd et al., 2013). Because melts from Haleakala are both relatively alkalic and crystallize deep within the lithosphere (Hammer et al., 2016), melt inclusions are more likely to trap a melt that is unaffected by significant degassing. Haleakala is therefore an ideal location to find recently-erupted and unmodified, primitive melt inclusions that sampled melts derived by partial melting of a volatile-enriched source. The goals of this study are to estimate the conditions under which degassing occurs in the "plumbing system" below Haleakala, to assess whether melt inclusions from Haleakala record evidence of a transition to a volatile-enriched plume source, and to apply information about the volatile content of the source material that is preserved by melt inclusions to improve upon existing models of Hawaiian island evolution.

2. Materials and methods

Ash and lapilli samples were collected from post-shield lava flows and monogenetic cinder cones at Haleakala Volcano on Maui, specifically targeting fresh, unaltered material that was likely to contain olivine phenocrysts. Fresh tephra samples were collected from Haleakala crater (Fig. 1), and lava samples were collected from Hana volcanic flows (Qhn6) on the southwestern coast of East Maui and from Lahaina Volcanic unit Qlhl on West Maui (Fig. 1 inset). Two of the tephra samples (HA-16-6 and HA-16-7; Hana volcanics) were found to contain abundant olivine phenocrysts containing glassy melt inclusions, and these samples were selected for melt inclusion analysis. GPS locations and sample description provided in Table S7 (Supplementary Materials).

Whole rock samples were crushed, washed in an ultrasonic bath with deionized water, and oven dried at 120 °C. Approximately 30 g of the cleaned bulk sample material was hand-picked under a binocular microscope to remove altered material and the cleaned material was analyzed for major and trace elements at Washington State University. Whole rock samples were analyzed using a combination of X-ray fluorescence (XRF) and solution inductively coupled plasma mass spectrometry (methods described by Johnson et al., 1999). New whole rock major and trace element compositions are listed in Supplementary Tables S1 and S2 respectively.

The remaining sample material was sieved to identify the grain size fraction containing the most abundant olivine grains, and these grains were hand-selected under a binocular microscope. All melt inclusions contained glass and fluid bubbles with some also containing small (<0.1 vol%) opaque particles that are likely sulfide globules or spinel crystals. Bubbles were analyzed by Raman spectroscopy at Virginia Tech using the methods described by Moore et al. (2015) and Lamadrid et al. (2017). Following Raman analyses, crystals containing melt inclusions were polished to expose the glass at the surface and pressed into a 1-in. diameter indium mount. Volatile concentrations of melt inclusion glasses were determined using Secondary Ion Mass Spectrometry (SIMS) at the Woods Hole Oceanographic Institute (methods described by Shimizu et al., 2009), and major element concentrations of melt inclusion glasses as well as host olivine grains were determined using electron probe microanalyses (EPMA) at Syracuse University. Finally, melt inclusion and host olivine grains were analyzed at Virginia Tech using laser ablation inductively coupled plasma mass spectrometry (LA-ICP-MS) to determine trace element concentrations. Melt inclusion and host olivine major and trace element compositions are listed in Supplementary Tables S3 and S4, respectively. Volatile contents of melt inclusions are listed in Supplementary Table S5.

Melt inclusion compositions were corrected for post-entrapment crystallization using the Petrolog3 program (Danyushevsky and

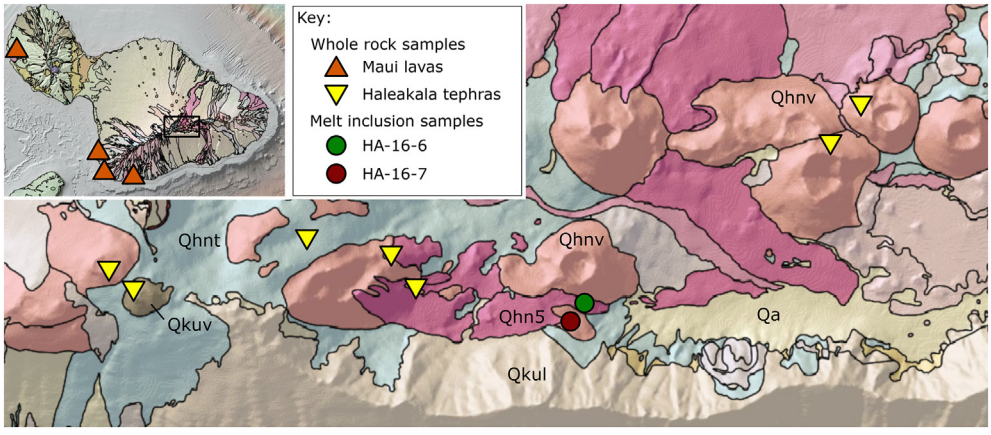

Fig. 1. Geologic map of sample locations. Geologic map and lithologic unit abbreviations after Sherrod et al. (2007). Hana volcanics: Qhnt - tephras, Qhnv - vent deposits, Qhn5 – lava flows; Kula volcanics: Qkuv – vent deposits, Qkul – lava flows; Qa: Holocene alluvium. Symbols indicate sample type as in Fig. 2.

Plechov, 2011). For these calculations, we used the Ford et al. (1983) olivine-melt model, the Lange and Carmichael (1990) melt density model, and a QFM buffer to control oxygen fugacity. To correct for Fe-loss, we used the total Fe concentration from whole rock analyses. Melt f_{O2} was estimated for melt inclusions using the V partitioning proxy described by Canil (2002).

After analyzing melt inclusions using LA-ICP-MS, we used the PEC-corrected Al_2O_3 concentration for each inclusion as the internal standard (normalizing element) so that the calculated trace element concentrations would reflect a PEC-corrected value (uncorrected trace element concentrations of melt inclusions are included in Supplementary Table S4). Because of the small size of the melt inclusions (~50 μm), and because the melt inclusions had been previously exposed to the surface by polishing, several of the laser ablation analyses included a mixture of glass and ablated host olivine, and these analyses were discarded as a precaution and because the LA-ICP-MS signal processing algorithm used in this study does not support deconvolution of a mixed host/inclusion signal.

Additional information regarding sample preparation and analytical methods is included in the supplementary methods description. Note that all reported melt inclusion compositions described in the results and discussion have been corrected for PEC and exsolution of CO_2 into bubbles except when stated otherwise.

3. Results

3.1. Major elements

Major element compositions of the whole rock samples are consistent with previously analyzed samples from Haleakala (Fig. 2) and with other Hawaiian post-shield-stage volcanoes. The compositions are alkalic and plot within the basalt, trachybasalt, and basanite fields on a total alkali vs silica (TAS) diagram (Fig. 2b). Forsterite contents [Fo# = 100 × molar Mg/(Mg + Fe)] of olivine host phenocrysts range from 68 to 87, and melt inclusions from one tephra sample (HA-16-6, host Fo# 79–87, mean = 82) are significantly more primitive than the other (HA-16-7, host Fo# 73–87, mean = 75). Melt inclusions generally experienced ~2–15% (interquartile range) post-entrapment crystallization (PEC), and inclusion major element compositions (after correcting for PEC) are consistent with the range of Haleakala whole rock compositions. An exception is that TiO_2 concentrations of melt inclusions (~1–3 wt%) are lower than those of the whole rocks (3–4 wt%).

3.2. Trace elements

Trace element concentrations of the lava and tephra whole rock samples are consistent with previous studies of Haleakala and other post-shield-stage volcanoes from Hawaii (Fig. 3). Both sample types are enriched in light rare earth elements (REEs), which is typical of an OIB derived from a low degree of partial melting. This is in contrast to melts from Haleakala's shield stage, which are generally interpreted to have originated from a higher degree of melting (Chen et al., 1991). Whole rock and melt inclusion samples also show depleted heavy REE concentrations, which are generally interpreted to reflect a garnet-bearing source (Hofmann et al., 1984; Wagner et al., 1998; Ren et al., 2004).

Trace element concentrations of melt inclusions and whole rock samples are similar (Fig. 3a) with melt inclusions from Haleakala sample HA-16-6 and Maui lava samples having lower REE concentrations compared to melt inclusions from Haleakala sample HA-16-7 and Haleakala tephra samples. Based on a similar relationship observed in our major element data, it is likely that this variation in light REE concentrations is due to differences in the degree of fractional crystallization. Light REE concentrations are also consistent with those observed

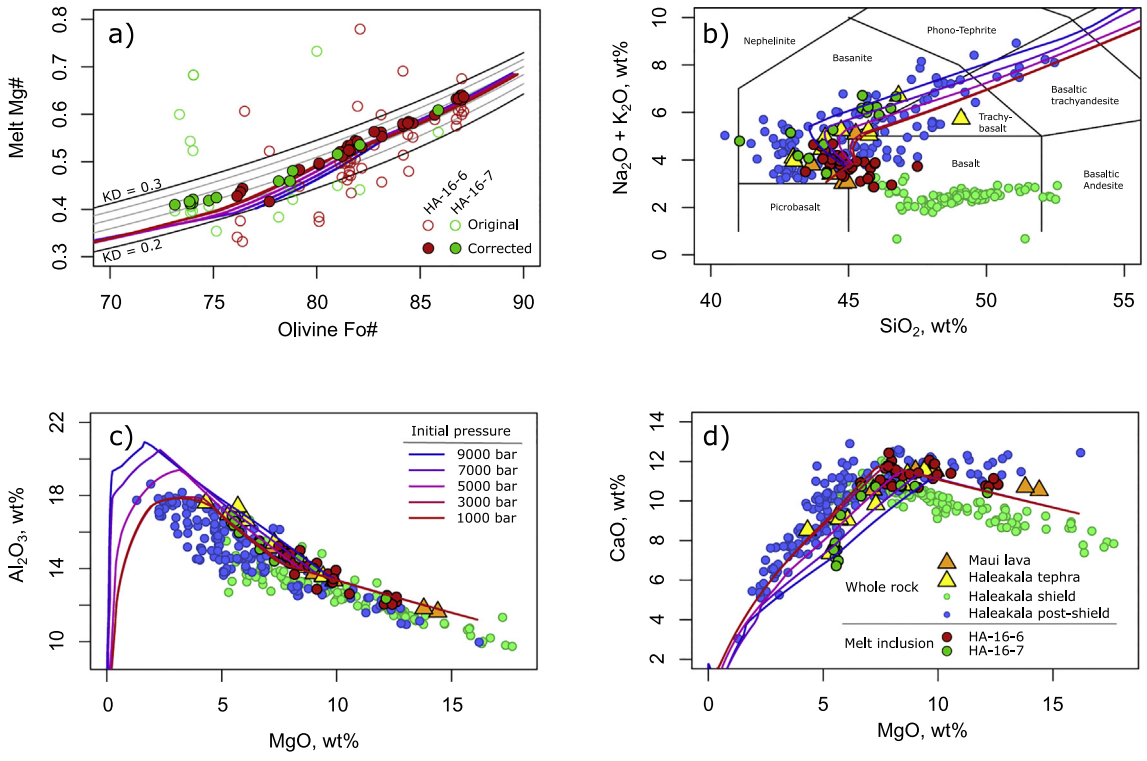

Fig. 2. Whole rock and melt inclusion compositions compared with MELTS models. Haleakala shield and post-shield stage whole rock compositions from GeoRoc database (http://georoc.mpch-mainz.gwdg.de/georoc/) are shown for comparison. a) Olivine host Fo# and melt inclusion Mg# used to correct for post-entrapment crystallization (PEC); all subsequent figures show compositions corrected for PEC only. b-d) comparison of melt inclusion, whole rock, and calculated liquid lines of descent (LLDs) reflect crystallization from a common parental melt with ~16 wt% MgO.

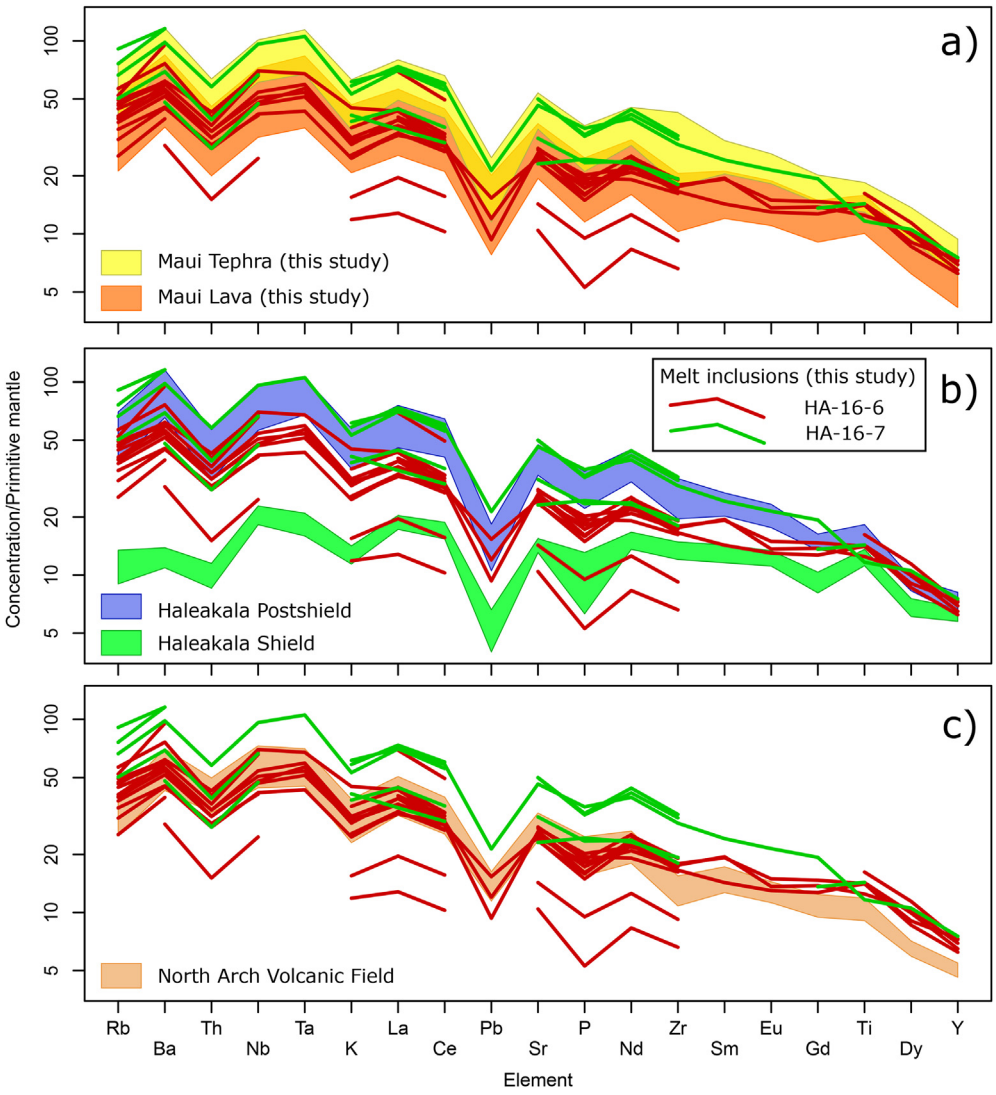

Fig. 3. Trace element compositions of melt inclusion samples HA-16-6 (red lines) and HA-16-7 (green lines) from Haleakala compared to a) whole rock lava (orange) and tephra (yellow) samples. b) shield stage (green), post-shield stage (blue), and c) North Arch Volcanic Field (NAVF) compositions (tan) compiled from the GeoRoc database are shown for comparison and filtered to show only the interquartile range.

from previously analyzed whole rock samples from Maui and intermediate between trace element compositions of previously-analyzed shield- and post-shield-stage lavas (Fig. 3b). Previously analyzed whole rock compositions from the NAVF (Fig. 3c) are similar to melt inclusions from Haleakala sample HA-16-6 but have more depleted heavy REE concentrations. This has been previously attributed to the presence of a garnet-bearing source in rejuvenated-stage lavas.

The melt inclusion trace element concentrations are significantly more variable than those of whole rocks, and two melt inclusions show consistently low trace element concentrations. It is not clear whether these anomalously depleted melt inclusion compositions are a result of olivine host contamination or evidence of a depleted melt composition similar to what has been previously reported for melt inclusions from Mauna Loa by Sobolev et al. (2011). Because the variability of the trace element abundances in melt inclusions increases with increasing compatibility in olivine, it is likely that some of the uncertainty may be related to contamination of the analytical volume by host olivine. Evaluating the effects of these processes on the observed heavy REE concentrations is beyond the scope of this study, and therefore we limit our discussion to exclude the heavy REE concentrations of individual melt inclusions.

3.3. Volatile components

Melt inclusions from Haleakala contain 500–2500 ppm F, 200–800 ppm Cl, 700–2500 ppm S, 0.2–1.2 wt% H_2O, and 0.3–1.3 wt% CO_2 (after correcting melt inclusion CO_2 compositions to account for exsolution into shrinkage bubbles, Fig. 4a). We note that other volatile components, such as S and H_2O, may have exsolved into fluid bubbles as has been reported previously (e.g. Esposito et al., 2016; Moore et al., 2018), but evidence of other exsolved components either as daughter crystals precipitated on the glass/fluid interface or as a component in the fluid was not observed during Raman analyses of the inclusions considered in this study. We also note that the CO_2-bearing fluid bubbles contained a mixture of liquid and vapor, and melt inclusions were analyzed at ~35 °C so that the fluid analyte would be homogenous during Raman analysis. Further details of this approach are discussed in the supplementary material.

To determine the extent to which the melt had degassed prior to trapping, melt inclusion volatile contents were compared to an incompatible element that is not likely to have been partitioned into a mineral or fluid phase given the compositional range over which olivine-hosted melt inclusions were being trapped. Fluorine was selected as the

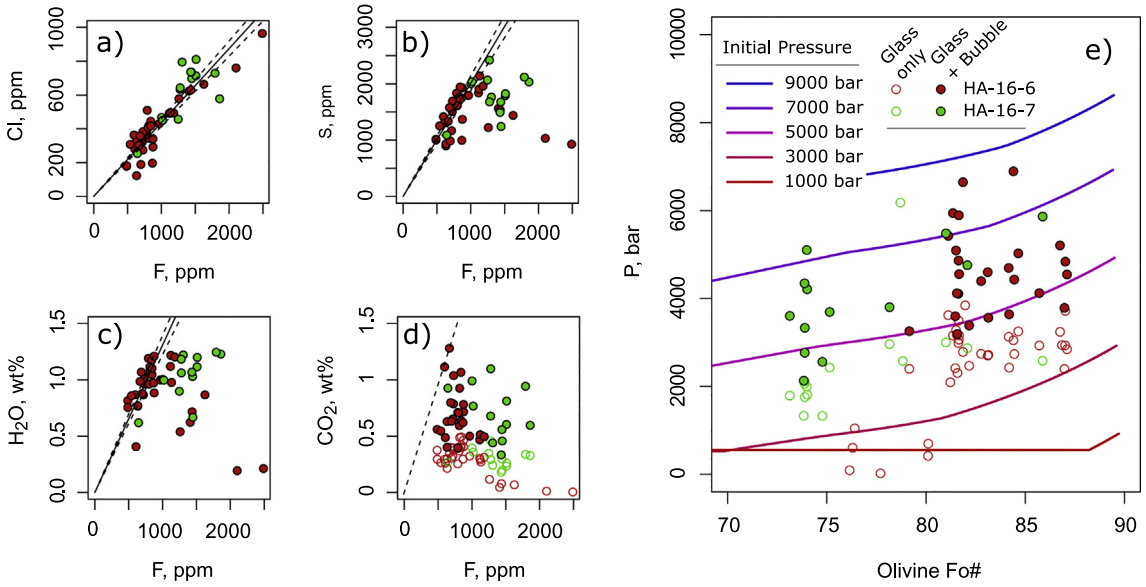

Fig. 4. (a–d) MI volatile concentrations with linear regression of presumably undegassed volatile concentrations indicating fractional crystallization. Light-colored symbols indicate MI glass compositions not corrected to include CO_2 exsolved into bubbles. A representative error bar is shown for CO_2 vs F. (e) Volatile-melt saturation pressures and MI host compositions compared with MELTS model results; pressures are calculated for each melt inclusion based on the trapping temperature and major element and volatile composition using the volatile-melt solubility model described by Iacono-Marziano et al. (2012).

incompatible element for comparison because it was collected simultaneously with the other volatile elements during SIMS analyses. Cl and F are highly correlated: it is therefore unlikely that the compositions of either of these elements were depleted by degassing during fractional crystallization (Fig. 4a). S and H_2O are well-correlated with F for inclusions with less than 1000 ppm F and poorly correlated for inclusions with greater than 1000 ppm F: we interpret this to indicate that both S and H_2O were initially enriched in the melt by fractional crystallization and then depleted by degassing when the melt became volatile-saturated (Fig. 4b, c). Additionally, the good correlation between H_2O and F suggests that melt inclusions experienced little diffusive loss of H_2O. Assessing whether CO_2 concentrations of melt inclusions were affected by degassing is more difficult because of the large (~50% relative) uncertainty associated with determining the volume of shrinkage bubbles petrographically (Moore et al., 2018; supplementary material). Thus, the variation in CO_2 (Fig. 4d) could potentially be explained either by propagated analytical error or by degassing, and additional information is required to determine whether the population of melt inclusions with F < 1000 ppm trapped a volatile-saturated melt.

The range of volatile contents that we determined is significantly larger than is observed for the shield stage. For comparison, Sides et al. (2014) report that melt inclusions from Kilauea contain to 0.8 wt % H_2O, up to 400 ppm F, 50–250 ppm Cl, and up to 1800 ppm S. Moore et al. (2015) report that melt inclusions from Kilauea contain up to 0.2 wt% CO_2 when the CO_2 contained in shrinkage bubbles is included. This difference in volatile abundances is likely related to a combination of melt inclusion trapping at greater depths (higher pressures), and a more alkalic melt composition. It is likely that the concentrations of (incompatible) volatile components in the melt would have been initially higher than those in the shield stage owing to a lower degree of partial melting or the participation of a different source, and then subsequently enriched by fractional crystallization. These processes are evaluated further, as described below.

3.4. Oxygen fugacity

To estimate the oxygen fugacity of melts from Haleakala, we used the olivine-melt V-partitioning oxybarometer described by Canil (2002), in which the oxygen fugacity of melts is correlated with the V olivine/melt partition coefficient (D_V). For melt inclusions from Haleakala, the range of D_V is ~0.02–0.04, which corresponds to approximately ΔQFM −1 to +0.5 (relative to quartz + fayalite + magnetite buffer at 1200 °C) or a ratio of ferric to total Fe ($Fe^{3+}/\Sigma Fe$) of 0.15 to 0.25 (Fig. 5a). This range is consistent with previous measurements of Fe speciation for Kilauea (Moussallam et al., 2016), Mauna Kea (Brounce et al., 2017), and the NAVF (Dixon, 1997). D_V is positively correlated with the composition of the host olivine (Fig. 5b), negatively correlated with incompatible elements F and S (Fig. 5c, d), and poorly correlated with volatile components H_2O, Cl, and CO_2. This suggests that the oxidation state of the melt, as recorded by the D_V proxy, is controlled by preferential incorporation of Fe^{2+} into crystallizing olivine, and is not significantly affected by degassing.

3.5. Parental melt composition modeling

To reconstruct the composition of parental melts derived from early melting of the mantle source below Haleakala, we used the silica activity thermobarometer of Lee et al. (2009) to incrementally add equilibrium olivine until the calculated melt composition is in equilibrium with mantle olivine. We used this model because it is more appropriate for low-SiO2 samples (<45 wt%; e.g. compared to PRIMELT; Herzberg and Asimow, 2008) and allows greater flexibility for multiple samples with variable H_2O contents. However, given the uncertainties associated with assessing equilibrium between potential source lithologies and our calculated parental melts, we evaluate whether our calculated parental melts are similar to other estimated primary melt compositions separately below (Sections 4.2 & 4.4). Samples with MgO < 8 wt% were excluded from the calculation to increase the likelihood that only melts crystallizing olivine would be used in our model. We assumed a molar Fe^{3+}/Fe_{total} = 0.2 based on the calculated fO_2 from the D_V oxybarometer described above, $K_d^{Fe/Mg}$= 0.3, and an assumed mantle Fo# = 90, which is consistent with the most primitive olivines from Maui (Ren et al., 2004). For whole rock samples, we assumed an H_2O concentration of 1.2 wt% based on the range of H_2O concentrations determined for melt inclusions, and calculated the composition of olivine that would precipitate using the correlation between melt inclusion

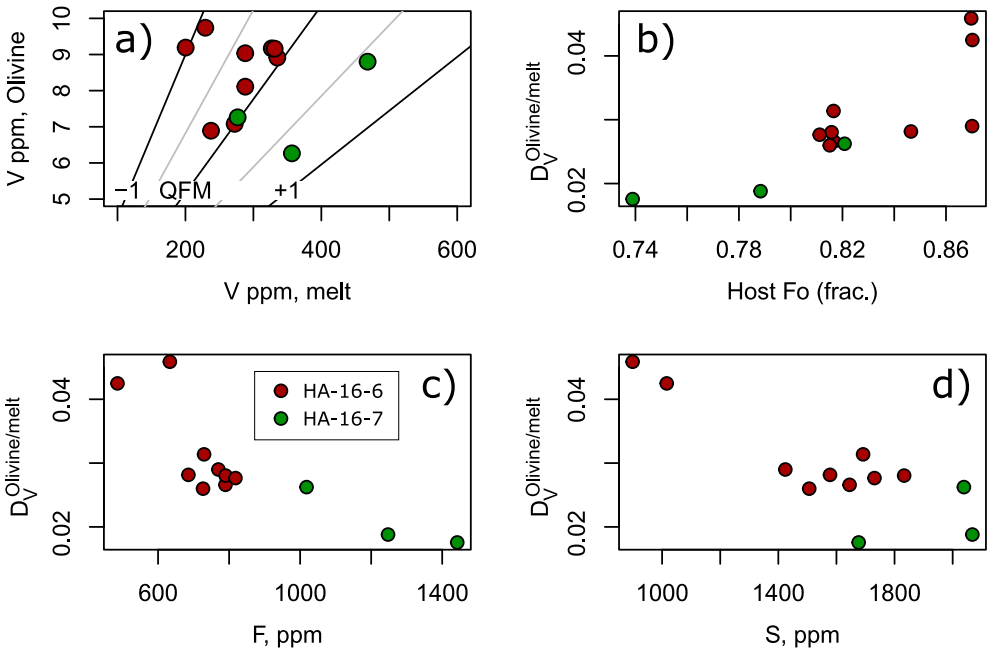

Fig. 5. Olivine-melt V partitioning and calculated oxidation state for melt inclusions from Haleakala. a) Contours of oxygen fugacity relative to quartz-fayalite-magnetite (QFM) buffer calculated using the relationship described by Canil (2002). D_V is positively correlated with host olivine forsterite content (b) and negatively correlated with F and S concentration in the glass.

host olivine composition and Al_2O_3 concentration. Parental melt compositions calculated from whole rock and melt inclusion samples are consistent, and indicate that ~5–30 wt% of olivine fractionation had occurred before melt inclusions were trapped. We used new mass of melt that is based on the calculated amount of olivine addition to the melt to correct volatile concentrations of primitive (MgO > 8) samples for olivine fractionation assuming perfect incompatibility with respect to the crystallizing melt. This assumption appears to be valid based on linear correlations observed between trace element concentrations and MgO concentration, and a lack of observed correlation between trace element ratios and MgO (Fig. 6). The observed input and calculated output compositions involved in this calculation are listed in Supplementary Table S6. Table 1 lists the average parental melt composition calculated using the Lee et al. (2009) thermobarometer, and this composition was used as the starting melt composition for the MELTS models of fractional crystallization described below. The average calculated volatile content of the parental melt is 400 ppm Cl, 1500 ppm S, 7000 ppm H_2O, and 7000 ppm CO_2. However, because of the likely possibility that CO_2

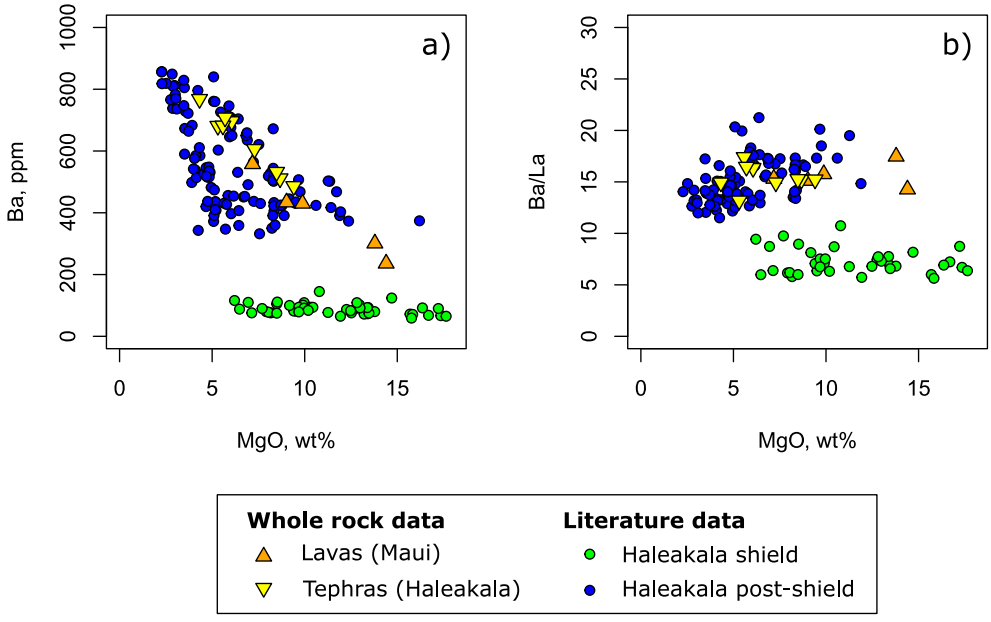

Fig. 6. Trace element concentrations in whole rock samples from Maui. Haleakala shield and post-shield stage whole rock compositions from GeoRoc database (http://georoc.mpch-mainz.gwdg.de/georoc/) are shown for comparison.

Table 1
Calculated parental melt composition.

SiO_2	TiO_2	$Al2O_3$	$Cr2O_3$	FeO	Fe_2O_3	MgO	MnO	CaO	Na_2O	K_2O	H_2O	CO_2
44.18	1.94	11.20	0.06	10.69	2.45	16.12	0.16	9.37	2.36	0.70	0.70	0.70

Oxide concentrations in wt%.

degassed from the melt before the melt inclusions analyzed in this study were trapped (discussed below), we note that the CO_2 concentration reported here reflects a minimum estimate.

4. Discussion

4.1. Mineral and fluid fractionation assessment

Previous studies of material erupted from Haleakala suggest that the observed range in major element compositions reflects olivine and pyroxene fractionation at various depths within the lithosphere (Bergmanis et al., 2000; Hammer et al., 2016). We used the program RhyoliteMELTS (Gualda et al., 2012) to calculate the range of major element compositions produced by fractional crystallization at conditions appropriate for the Haleakala system. Melt liquid lines of descent (LLDs) were calculated using the parental composition shown in Table 1 and an oxygen fugacity buffered by QFM (within the range estimated using D_V). The starting pressures for the calculations were 3, 5, 7, and 9 kbar (corresponding to approximately 10 to 30 km depth), with a decompression gradient of 75 bar/°C. This range of gradients was selected 1) because of an observed correlation between host Fo# and calculated trapping pressure (discussed below) and 2) on account of good agreement between observed and modeled melt major element concentrations and host Fo#. Of the various input parameters, the trajectory of the LLDs for a given parental melt composition was most dependent on the initial pressure and decompression rate, while the initial H_2O concentration of the melt and oxygen fugacity had a minimal impact on the results.

To compare the melt inclusion trapping conditions to the conditions simulated by the model, we used the volatile-melt solubility model of Iacono-Marziano et al. (2012), which is calibrated for alkaline melt compositions similar to those observed in this study, to calculate saturation pressures for each melt inclusion as a function of the major element and volatile composition and compared the results to other pressure constraints. Calculated volatile-melt saturation pressures are ~2 to 7 kbar, which correspond to depths of ~7 to 24 km assuming a 3.5 km/kbar lithostatic pressure gradient. The volatile-melt saturation pressures that we calculate for our melt inclusions are correlated with the forsterite contents of the phenocrysts which host them, and this correlation can be directly compared to the LLDs calculated using RhyoliteMELTS. The LLDs showing olivine composition as a function of pressure calculated based on a 75 bar/°C decompression gradient from 3 and 5 kbar starting pressures are consistent with the range of inclusion/host pairs (Fig. 4e). Because the crystallization model is both dependent on pressure and consistent with the major element compositions of the whole rock and melt inclusion samples that we have analyzed, it is likely that the pressures supplied to the model are valid.

To further evaluate the validity of our calculated trapping pressures, we compare our fractional crystallization modeling results and calculated volatile-melt saturation pressures to previous results reported for Haleakala. Previous studies have used petrologic modeling (Bergmanis et al., 2000) and clinopyroxene geobarometry (Chatterjee et al., 2005; Hammer et al., 2016) to determine crystallization depths for magma reservoirs in the lithosphere below Haleakala. Based on petrologic modeling, Bergmanis et al. (2000) report crystallization pressures of ~3 kbar, but Chatterjee et al. (2005) report pyroxene crystallization pressures up to 10 kbar. More recently, Hammer et al. (2016) used an X-ray mapping technique to relate calculated trapping pressures to petrographic features within individual clinopyroxene phenocrysts and grain morphology and report a range of saturation pressures from 3.6 to 7.1 kbar. Furthermore, Hammer et al. (2016) also demonstrate that pressures obtained from pyroxene geobarometry are highly model-dependent, and pyroxene/melt compositions reported by Hammer et al. (2016) and by Chatterjee et al. (2005) yield mutually consistent pressures (up to ~9.5 kbar) when the same model is used.

The range of pressures obtained from pyroxene geobarometry and petrologic modeling described above is consistent with our petrologic modeling results and volatile-melt saturation pressures based on melt inclusions. We also note that the range of pyroxene Mg# for pyroxenes analyzed by Hammer et al. (2016) is consistent with the range of olivine host Fo# observed in this study. Thus, the mutual consistency between calculated volatile-melt saturation pressures, pyroxene crystallization pressures, and the observed and modeled range of major element compositions (which are also a function of pressure) strongly suggests that the volatile-melt saturation pressures reflect melt inclusion trapping pressures. If this is the case, then the melt trapped by the melt inclusions must have been volatile-saturated, and it is likely that the volatile concentrations that we report represent the concentrations after some portion of the original volatile budget was lost through degassing.

4.2. Melting and source H_2O content

Given the melt inclusion volatile contents presented in this study, the volatile content of the source can be constrained based on bulk mineral/melt partitioning behavior of volatiles and an assumed degree of melting. While the link between melt inclusion CO_2 and source composition is tenuous owing to the likelihood of significant degassing, the correlation between H_2O and other incompatible elements (e.g. fluorine, Fig. 4) suggests that some of the melt inclusions (<1000 ppm F) were trapped before a significant amount of H_2O had exsolved from the melt, and therefore estimation of the source H_2O concentration is possible provided that the necessary melting parameters can be constrained. The uncertainty associated with the estimated degree of melting, which has been estimated previously for the shield, post-shield, and rejuvenated stages propagates to a large degree of uncertainty in the calculated source volatile contents (Table 2). Although constraining mineral/melt partitioning behavior is non-trivial, bulk mineral/melt partitioning behavior of H_2O is relatively well-constrained for peridotite ($D_{H_2O} \approx 0.01$; Aubaud et al., 2004), and the overall uncertainty of the source volatile content is dominated by uncertainty associated with the degree of melting because of the highly incompatible nature of the volatile elements in mantle lithologies.

Based on these parameters, we can calculate the H_2O concentration of the source material that melted to produce the shield and post-shield stages for comparison. Using the relationship between K_2O and degree of melting proposed by Dixon et al. (1997), the degree of melting experienced by the primary melts calculated in this study were generated as a result of approximately 6.5 to 8% partial melting of the source material (Chen et al., 1991). Using this degree of melting and a bulk partition coefficient $D_{H_2O}^{Peridotite/melt} = 0.011$, we calculate that the minimum primary melt H_2O concentration inferred from our analyses of melt inclusions (~0.7 wt%) could be produced by melting a source containing 580 ± 50 ppm H_2O. Previous analyses of seafloor basalts (Dixon et al., 1997) imply that the primary melt would have had a CO_2/H_2O ratio of

Table 2
Calculated source H_2O concentrations.

Location	Stage	Reference	Primary melt H2O (wt%)	Melt fraction (%)	Mantle H_2O (ppm)
Loihi	Tholeiite	Dixon and Clague (2001)	~0.3	10	~400
Kilauea	Tholeiite	Clague et al. (1991)	0.35	8 to 10	350 ± 35
Kilauea	Tholeiite	Wallace and Anderson (1998)	0.4	5 to 10	350 ± 100
Mauna Kea	Tholeiite	Herzberg & Asimow (2008)	0.2 to 0.4	5 to 25	460 ± 280
Haleakala	Alkali basalt	This study, Chen et al. (1991)	~0.7	6.5 to 8	580 ± 50
North Arch	Alkali basalt	Dixon et al. (1997)	0.5 to 2.0	1.6 to 9	525 ± 75
Rejuvenated stage (Model 1)	Alkali basalt	Dixon et al. (2008)	0.3 to 1.2	1 to 9	255
Rejuvenated stage (Model 2)	Alkali basalt	Dixon et al. (2008)	0.5 to 2.6	1 to 9	540

about 2.5, which provides a means to estimate the source CO_2 concentration alternative to using the CO_2 content of melt inclusions, which were likely trapped after degassing of a CO_2-rich vapor had occurred. Using the a CO_2/H_2O ratio of 2.5, the calculated primary melt CO_2 concentration would be 1.75 wt%, which yields a source CO_2 concentration for Haleakala of approximately 1760 ppm based on a bulk partition coefficient of $D_{CO_2}^{Peridotite/melt} = 0.00055 \pm 0.00025$ (Rosenthal et al., 2015).

Our results are consistent with the range of volatile contents estimated previously for the sources of rejuvenated stage magmas (Dixon et al., 2008; Table 2) which range from approximately 255 ppm to 540 ppm H_2O depending on the degree of mixing between a Hawaiian mantle component, incipient silicic melts produced by different extents of previous melting, and the addition of deeply sourced carbonatitic fluids. Similarly, previous studies have estimated the source volatile content associated with the shield melting stage at the center of the plume. These include 350 ± 100 ppm H_2O for Kilauea (Clague et al., 1991; Wallace and Anderson, 1998) estimated based on ~5–10% melting, and approximately 400 ppm H_2O for submarine (pre-shield stage) lavas at Loihi based on a model with 10% melting (Dixon and Clague, 2001). The source H_2O concentration that we calculate is intermediate between the enriched concentrations for the rejuvenated stage (e.g. "Model 2" from Dixon et al., 2008) and the North Arch Volcanic Field and the relatively depleted H_2O concentrations associated with Kilauea and Loihi. This result is consistent with the trace element concentrations of our whole rock and melt inclusion samples (Fig. 3b), which are also intermediate between shield- and rejuvenated-stage compositions. In contrast, petrologic modeling by Herzberg and Asimow (2008) suggests that the degree of melting varies substantially over short distances (~10s of km), and the degree of melting could be 5–25% at the center of the plume. Using this higher degree of melting implies that the source volatile content associated with the shield stage could contain 460 ± 280 H_2O. This example illustrates that the high degree of uncertainty associated with estimating the melt fraction and the sensitivity of the calculated source volatile content to that parameter limits our ability to make direct comparisons of the volatile content between different source materials.

4.3. Source composition constraints from volatile component/trace element ratios

Ratios of volatile components and incompatible trace elements are useful for comparing the volatile contents of melts derived from different environments that may have experienced different degrees of partial melting. H_2O is thought to have a bulk solid/melt partition coefficient that is similar to that of Ce (Michael, 1995), and Nb is thought to behave similarly to CO_2 (Saal et al., 2002) However, more recent experimental evidence suggests that CO_2 may be more incompatible than Nb and have an average mineral/melt partition coefficient in basalts that is closer to that of Ba (Rosenthal et al., 2015). Regardless, given that the bulk melt partition coefficients of these volatile/trace element pairs are similar, it is possible to compare the volatile contents of different melt sources in a manner that is not affected by different degrees of melting and crystal fractionation by normalizing volatile elements to an incompatible element with a similar solid/melt partition coefficient. However, volatile/trace element ratios of melt inclusions from Haleakala (Fig. 7) are positively correlated with the forsterite content of the olivine. We do not observe a significant correlation between the forsterite content of host olivine crystals and the H_2O and CO_2 contents of melt inclusions owing to both a variable amount of H_2O partitioning into the fluid phase (Fig. 4c) and a significant amount of scatter in CO_2 concentrations due to degassing and/or the high degree of relative uncertainty associated with quantifying CO_2 in vapor bubbles (Fig. 4d). Therefore, the correlation between volatile/trace element ratios is likely to be a result of enrichment of Ce, Nb, and Ba in the melt by crystal fractionation (i.e. affecting the numerator as opposed to the denominator in the ratio). Regardless of the cause, the correlation with Fo# suggests that the assumption that these ratios are unaffected by crystal fractionation may not be entirely appropriate in this case and that the volatile/trace element ratios of our most primitive melt inclusions are the most suitable for comparison to other inclusions potentially derived from different source compositions.

Volatile/trace element ratios of melt inclusions from Haleakala presented in this study are compared to similar data from Hawaii and Iceland, which represent the two most well characterized OIB locations where undegassed melt volatile/trace element ratios have been reported. Tucker et al. (2019) present a dataset of melt inclusion CO_2/Ba and CO_2/Nb ratios from several Hawaiian islands; these compositions were corrected for the presence of CO_2 contained in shrinkage bubbles using an equation of state. As yet, no other studies from Hawaii present CO_2/trace element ratios in melt inclusions which have been corrected using in situ analysis of shrinkage bubbles with Raman spectroscopy, so we also compare our results to a combination of melt inclusion data from the 1959 Kilauea Iki eruption which includes 1) melt inclusion glasses in which CO_2, Ba, and Nb concentrations were measured (Sides et al., 2014), and 2) CO_2 contents of shrinkage bubbles determined using in situ Raman analyses (Moore et al., 2015). To provide further comparison with glasses dredged from the NAVF, which represent some of the most well-characterized samples of volatile-rich submarine lavas in Hawaii, we calculate volatile/trace element ratios using trace elements reported by Frey et al. (2000) and undegassed volatile element concentrations reported by Dixon et al. (1997). Additionally, we include H_2O/Ce ratios from Kaua'i-Oahu channel (KOC) submarine glass samples (Samples 2D and 4D; J. Dixon, personal communication), which approximate the volatile content of rejuvenated-stage lavas. Finally, we also consider our results within the context of a growing dataset of estimated mantle volatile/trace element ratios, including 14°N mid-atlantic ridge (MAR; Cartigny et al., 2008), Pacific mid-ocean ridge basalt from the East Pacific Rise (EPR; Shimizu et al., 2016), and Borgarhraun (Northern Iceland; Hauri et al., 2018).

Melt inclusions from Haleakala have an average H_2O/Ce ratio of ~200, which is consistent with KOC glasses 2D and 4D (211 and 188 respectively), 14°N MAR, and EPR; and higher than average H_2O/Ce ratios of shield-stage melt inclusions from Kilauea (Sides et al., 2014; ~100) by a factor of 2. H_2O/Ce is correlated with host Fo content and approaches an average value of ~400 at the host olivine composition Fo# = 90

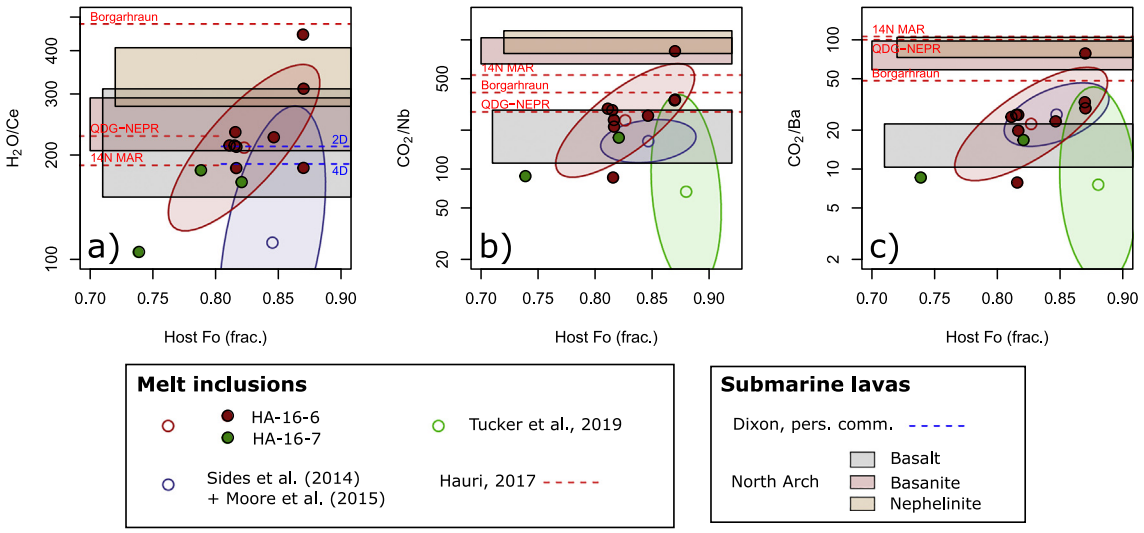

Fig. 7. Volatile/light rare earth element ratios of melt inclusions and submarine lavas from Hawaii and Pacific lithosphere. Shaded ellipses show the 1σ probability interval for the mean composition of each sample population as indicated by the open circle at the center. Horizontal lines indicate volatile/trace ratios of presumably undegassed melts reported by Hauri et al. (2018). Shaded horizontal bars show the range of compositions from dredged North Arch lavas using trace element compositions reported by Frey et al. (1990) and volatile element concentrations estimated by Dixon et al. (1997) for alkali olivine basalts (gray), basanites (pink), and nephelinites (orange). Also shown for comparison are (a-c) melt inclusion compositions from Kilauea using glass volatile and trace element concentrations from Sides et al. (2014), which have been corrected assuming a contribution of 2000 ppm of additional CO_2 from the bubble (Moore et al., 2015), and (b–c) melt inclusion volatile/trace element ratios from several Hawaiian volcanoes reported by Tucker et al. (2019) which have been corrected to account for bubbles using an equation of state. The dark gray rectangle shows the compositional range of EPR host olivine and melt inclusions reported by Wanless and Shaw (2012) based on the interquartile range of Ce, Nb, Ba, H_2O and host Fo concentrations, and the upper quartile of CO_2 concentrations.

(Fig. 7a), which is consistent with the range predicted by undegassed nephelinite North Arch melts (approximately 300–400) and lower than the H_2O/Ce for Borgarhraun.

Similarly, CO_2/Nb ratios for our melt inclusions are higher on average than previous reported values for Hawaii reported by Sides et al. (2014), Moore et al. (2015), and Tucker et al. (2019). Correlated with Fo#, melt inclusion CO_2/Nb ratios approach a value of ~500 (Fig. 7b) which is consistent with Borgarhraun, 14°N MAR, and NAVF basanites and nephelinites, and higher than EPR and NAVF basalts. In contrast, CO_2/Ba ratios for our melt inclusions are nearly identical to the corrected range for Kilauea Iki (Sides et al., 2014; Moore et al., 2015) and closer to the range of CO_2/Ba reported by Tucker et al. (2019). CO_2/Ba ratios of melt inclusions from Haleakala are also correlated with host Fo# and approach ~70, which is consistent with the range of NAVF submarine lavas and samples from Borgarhraun, 14°N MAR, and EPR. We note that the inconsistency in relative CO_2/Ba and CO_2/Nb contents may be due to differences in the relative compatibility of CO_2 and Nb (as discussed by Rosenthal et al., 2015) and could be related to differences in the degree of melting between Haleakala and Kilauea.

Although the method of comparing volatile/trace element ratios is advantageous because it provides a means to control for variations in the extent of melting and crystallization, it is still challenging to draw conclusions about the relative CO_2 content of the source material because of the potential effect of magmatic degassing which affect CO_2/Nb and CO_2/Ba. Specifically, these effects include differences in magma storage depth, and/or compositional variations which influence volatile solubility. With increasing age and distance from the plume center, magma chambers in the Hawaiian volcanoes are thought to occur at greater depths (Clague and Sherrod, 2014); on this basis, crystallizing magma stored below Haleakala is more likely to trap melt inclusions with higher CO_2/Nb and CO_2/Ba compared to Kilauea even with the same primary melt CO_2 concentration. Additionally, CO_2 is significantly more soluble in alkaline melts than in tholeiitic melts (Dixon et al., 1995, 1997), and therefore melts from Haleakala have the potential to hold more CO_2 than more silicic shield stage melts from Kilauea even at the same pressure. Thus, the magmatic conditions present at Haleakala (alkaline melts; deep fractionation) permit fluid-saturated melts to have higher CO_2/trace element ratios than those likely to occur in melt inclusions from Kilauea (relatively silicic melts; shallow fractionation), and there is insufficient evidence to reject the simple hypothesis that the CO_2/trace element ratios that we observe are controlled by the limit of shallow degassing and fractional crystallization in favor of an alternative hypothesis that the elevated CO_2/trace element ratios at Haleakala are also influenced by differences in the melting environment.

In contrast, because of the correlation between H_2O and F observed among our less fractionated melt inclusion samples (Fig. 4c), it is less likely that the H_2O content of our inclusions is dominated by magmatic processes, and more robust comparisons can be made between source H_2O/Ce contents of Haleakala and other localities. The observation that melt inclusions from Haleakala have intermediate H_2O/Ce ratios between melt inclusions from Kilauea and undegassed NAVF submarine glasses is consistent with a scenario in which Haleakala is partially influenced by the H_2O-enriched auto-metasomatized periphery of the Hawaiian plume (e.g. Dixon and Clague, 2001).

While CO_2/Nb and CO_2/Ba ratios of melt inclusions from Haleakala do not provide definitive information about variations in the source composition, these ratios can alternatively be used to estimate and correct for the potential effect of CO_2 loss due to degassing. This approach requires the use of an undegassed volatile/trace element ratio obtained from an undegassed melt (e.g. Sides et al., 2014; Longpre et al., 2017; Hauri et al., 2018). In this case, we used the Ba concentrations of our melt inclusions and an assumed primary CO_2/Ba ratio of 48.3 reported by Hauri et al. (2018) to estimate the amount of CO_2 that would be present in the undegassed primary melt. This approach yields a range of calculated CO_2 concentrations from approximately 1–2 wt%. Given a primary CO_2/H_2O ratio of 2.5 as reported by Dixon et al. (1997), this range of primary CO_2 corresponds to a primary melt H_2O concentration of approximately 0.4–0.8 wt%, which is consistent with the 0.7 wt% H_2O that we calculated using the model from Lee et al. (2009). However, this range of CO_2 concentrations is significantly higher than the parental melt CO_2 concentration of 0.7 wt% estimated above, and suggests that approximately 30–70% of the primary CO_2 content has been lost to degassing.

An alternative possibility to degassing is that the melt inclusions originally trapped a more CO_2-rich melt, but lost CO_2 by systematic decrepitation as a result of inclusion overpressure during ascent to shallower depths in the lithosphere. This process has been invoked to explain why volatile-melt saturation pressures calculated from melt inclusions tend to systematically underestimate saturation pressures calculated from pyroxene thermobarometry (Maclennan, 2017). Without additional information, this possibility is difficult to assess depending on the extent to which decrepitation features, such as "haloes" of melt and fluid inclusions (e.g. Sterner et al., 1995; Bodnar and Student, 2006) or radial fractures surrounding melt inclusions – neither of which we observed adjacent to melt inclusions reported in this study – are able to anneal following decrepitation. As described above, volatile-melt saturation pressures calculated in this study are consistent with independently-calculated pressures from pyroxene thermobarometry (Hammer et al., 2016). This suggests that the melt inclusions in this study have not lost CO_2 due to decrepitation.

4.4. CO_2 in silica undersaturated melts

As an alternative to the geochemical methods described in the previous section, direct comparison with experimentally derived melts provides another means by which the original volatile content of the melt may be estimated. Experimental evidence suggests that low-silica alkalic OIBs, such as those erupted at Haleakala, can be potentially derived by partial melting of a carbonated ultramafic source material. While the presence of relatively silica-poor, alkaline melts may not be a sufficient condition to infer the presence of a CO_2-rich parental melt, experimental melts produced from a carbonated source material represent the only petrologically viable primary melt composition to date that could fractionate to produce relatively low-SiO_2 (≤45 wt%) OIB-like melt compositions (Eggler, 1978; Edgar, 1987; Hémond et al., 1994; Dasgupta et al., 2007). For this reason, the major element compositions of the samples analyzed in this study suggest the influence of a CO_2-rich primary melt and mantle source. To explore this possibility, we compared the major element compositions of the parental melts calculated using the Lee et al. (2009) thermobarometer to a compilation of data from experimental carbonated peridotite melting experiments (Dasgupta et al., 2004; Dasgupta et al., 2007; Dasgupta et al., 2013), which we have parameterized using a multiple linear regression model (Supplementary Material). Using this approach, the calculated primary CO_2 concentration in the melt is approximately 8.0 ± 5 wt% (2σ). For comparison, we also used this approach to calculate the primary melt CO_2 concentration associated with Mauna Kea using primary melt compositions reported by Herzberg and Gazel (2009). Primary melt CO_2 concentrations calculated for Mauna Kea contain approximately 5.5 ± 5 wt% (2σ) and are lower on average than those calculated for Haleakala (Fig. 8).

Interpreting this result is challenging owing to both the high amount of uncertainty from the lack of constraints on the pressure and temperature conditions at which melting occurred as well as the appropriateness of directly comparing these particular experimental data to our inferred primary melt compositions. Therefore, we interpret the calculated CO_2 concentrations above to reflect differences in the capacity of the melts to contain CO_2 rather than the actual primary melt CO_2 concentration. This variation in the calculated CO_2 concentration also does not imply differences in the source composition and instead likely reflects a difference in the degree of melting at each location (Haleakala: ~5%; Mauna Kea: ~15%). We also note that, given the ~0.7 wt% H_2O that we estimated above, which is consistent with the primary CO_2 content estimated using a presumably undegassed CO_2/Ba ratio from Hauri et al. (2018), a primary melt composition of 8.0 ± 5 wt% requires a CO_2/H_2O ratio of approximately 2–9 which is consistent with the value of 2.5 ± 1.5 estimated by Dixon et al. (1997), and suggests that the CO2/H2O ratio could be significantly greater. Alternatively, a discrepancy between the

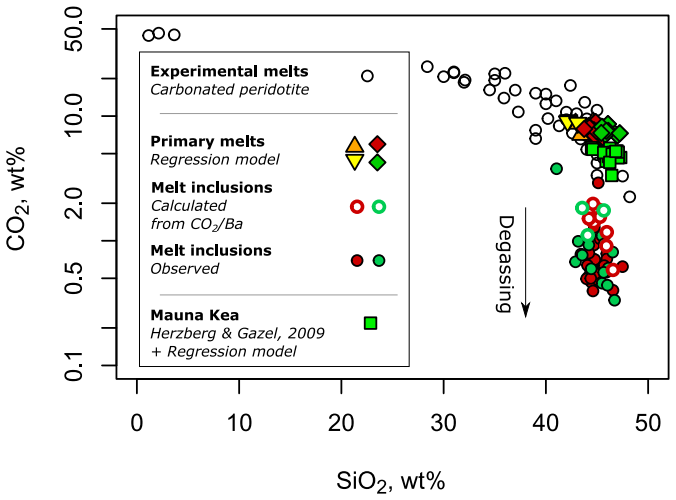

Fig. 8. Primary melt CO_2 concentrations calculated based on carbonated peridotite melting experiments. CO_2 concentrations were calculated from Haleakala and Mauna Kea primary melt compositions and experimental data using a multiple linear regression model (see Supplementary Methods for details). Also shown are CO_2 concentrations calculated for Haleakala melt inclusions using a primary CO_2/Ba ratio of 48.5 (Hauri et al., 2018).

CO_2/H_2O ratio stated above (2–9) and the value estimated by Dixon et al. (1997) could be explained by either case where 1) primary melts below Haleakala contain significantly less CO_2 than was in the experimentally-derived melts, 2) the assumed mantle CO_2/Ba ratio used for the calculation does not describe the mantle source associated with Haleakala's post-shield volcanism, or 3) the calculated parental melt composition is inaccurate. As discussed by Rosenthal et al. (2015), mineral/melt partitioning of CO_2 likely depends on melt composition, and it is possible that the CO_2 concentrations in melts used by Hauri et al. (2018) to estimate the source CO_2/Ba ratio may not be appropriate for melts from Haleakala, which are significantly more alkaline than those considered by Hauri et al. (2018).With this in mind, we interpret the result that calculated CO_2 concentrations from Haleakala are greater than those from Mauna Kea to be consistent with the previously proposed model in which the outer portion of the Hawaiian plume is more likely to preserve relatively volatile-rich source material that has been previously auto-metasomatized by CO_2-rich fluids.

5. Conclusions

We analyzed olivine-hosted melt inclusions from Haleakala volcano (Hawaii) to estimate the pre-eruptive volatile content and melting and crystallization conditions at the periphery of the Hawaiian plume. Melt inclusions record evidence of volatile-saturated, polybaric fractional crystallization starting at pressures of 5–7 kbar. We estimate that the parental melt contains approximately 400 ppm Cl, 1500 ppm S, 0.7 wt % H_2O, and 0.7 wt% CO_2, but note that the estimated CO_2 concentration may have been significantly affected by degassing of CO_2 before melt inclusion entrapment and therefore reflects a minimum concentration.

Melt inclusions from Haleakala have H_2O/Ce and CO_2/Nb ratios significantly higher than melt inclusions from Kilauea and EPR lavas, and these observations suggest that melts from Haleakala's post-shield stage are derived from a more H_2O- and CO_2-rich melt source than the shield stage or Pacific ambient mantle. This is consistent with a scenario in which the composition of post-shield melts from Haleakala are transitional between an isotopically enriched, volatile-poor shield component and an isotopically depleted, volatile-rich rejuvenated component.

Supplementary data to this article can be found online at https://doi.org/10.1016/j.jvolgeores.2020.107144.

Declaration of Competing Interest

The authors declare that they have no known competing financial interests or personal relationships that could have appeared to influence the work reported in this paper.

Acknowledgements

This work was supported by National Science Foundation grants EAR 1802012 and OCE 1756349 to EG, EAR-1624589 and OCE-1634211 to RJB, and a Geological Society of America graduate student research grant to LRM. Samples were collected under the study HALE-00134 and permit HALE-2016-SVI-0004 of the Haleakala National Park, United States Department of the Interior, National Park Services. There authors are grateful for the field support by the staff of the Haleakala National Park. The authors wish to thank Brian Monteleone for assistance with SIMS analyses, Jay Thomas and Will Nachlas for assistance with EPMA, and Luca Fedele and Eszter Sendula for assistance with LA-ICP-MS analyses. The authors also wish to thank three anonymous reviewers, Jaqueline Dixon, and Tom Sisson for reviews of earlier versions of this manuscript.

Appendix A. Supplementary data

Supplementary data to this article can be found online at https://doi.org/10.1016/j.jvolgeores.2020.107144.

References

Abouchami, W., Hoffmann, A.W., Galer, S.J.G., Frey, F.A., Eisele, J., Feigenson, M., 2005. Lead isotopes reveal bilateral asymmetry and vertical continuity in the Hawaiian mantle plume. Nature 434, 851–856.

Anderson, A.T., Brown, G.G., 1993. CO_2 contents and formation pressures of some Kilauean melt inclusions. Am. Mineral. 78, 794–803.

Aster, E.M., Wallace, P.J., Moore, L.R., Watkins, J., Gazel, E., Bodnar, R.J., 2016. Reconstructing CO2 concentrations in basaltic melt inclusions using Raman analysis of vapor bubbles. JVGR 323, 148–162.

Aubaud, C., Hauri, E.H., Hirschmann, M.M., 2004. Hydrogen partition coefficients between nominally anhydrous minerals and basaltic melts. Geophys. Res. Lett. 31 (L20611), 1–4.

Ballmer, M.D., Ito, G., Wolfe, D.J., Solomon, S.C., 2013. Double layering of a thermochemical plume in the upper mantle beneath Hawaii. Earth Planet. Sci. Lett. 376, 155–164.

Bergmanis, E.C., Sinton, J.M., Trusdell, F.A., 2000. Rejuvenated volcanism along the southwest rift zone, East Maui, Hawai'I. Bull. Volcanol. 62 (4–5), 239–255.

Bianco, T.A., Ito, G., Becker, J.M., Garcia, M.O., 2005. Secondary Hawaiian volcanism formed by flexural arch decompression. Geochem. Geophys. Geosyst. 6 (8), 1–24.

Bizimis, M., Salters, V.J.M., Garcia, M.O., Norman, M.D., 2013. The composition and distribution of the rejuvenated component across the Hawaiian plume: Hf-Nd-Sr-Pb isotope systematics of Kaula lavas and pyroxenite xenoliths. Geochem. Geophys. Geosyst. 14 (10), 4458–4478.

Blichert-Toft, J., Weis, D., Maerschalk, C., Agranier, A., Albarède, F., 2003. Hawaiian hot spot dynamics as inferred from the Hf and Pb isotope evolution of Mauna Kea volcano. Geochem. Geophys. Geosyst. 4 (2), 1–27.

Bodnar, R.J., Student, J.J., 2006. Melt inclusions in plutonic rocks: Petrography and microthermometry. In: Webster, J.D. (Ed.), Melt Inclusions in Plutonic Rocks. vol. 36. Mineral. Assoc., Canada, pp. 1–26 (Short Course).

Brounce, M., Stolper, E., Eiler, J., 2017. Redox variations in Mauna Kea lavas, the oxygen fugacity of the Hawaiian plume, and the role of volcanic gases in Earth's oxygenation. PNAS 114 (34), 8997–9002.

Canil, D., 2002. Vanadium in peridotites, mantle redox and tectonic environments: Archean to present. Earth Planet. Sci. Lett. 195, 75–90.

Cartigny, P., Pineau, F., Aubaud, C., Javoy, M., 2008. Towards a consistent mantle carbon flux estimate: Insights from volatile systematics (H2O/Ce, δD, CO2/Nb) in the North Atlantic mantle (14° N and 34° N). Earth Planet. Sci. Lett. 265 (3–4), 672–685.

Chatterjee, N., Bhattacharji, S., Fein, C., 2005. Depth of alkalic magma reservoirs below Kolekole cinder cone,Southwest rift zone, East Maui, Hawaii. J. Volcanol. Geotherm. Res. 145, 1–22.

Chen, C.-Y., Frey, F.A., Carcia, M.O., Dalyrimple, G.B., Hart, S.R., 1991. The tholeiite to alkalic basalt transition at Haleakala Volcano, Maui, Hawaii. Contrib. Mineral. Petrol. 106, 183–200.

Clague, D.A., Dalrymple, G.B., 1987. The Hawaiian-emperor volcanic chain. U. S. Geol. Surv. Prof. Pap. 1350, 5–54.

Clague, D.A., Sherrod, D.R., 2014. Growth and degradation of Hawaiian volcanoes. US Geol. Surv. Prof. Pap. 1801, 97–146.

Clague, D.A., Weber, W.S., Dixon, J.E., 1991. Picritic glasses from Hawaii. Nature 353, 553–556.

Danyushevsky, L.V., Plechov, P., 2011. Petrolog3: integrated software for modeling crystallization processes. Geochem. Geophys. Geosyst. 12 (7) (32 pp.).

Danyushevsky, L.V., McNeill, A.W., Sobolev, A.V., 2002. Experimental and petrological studies of melt inclusions in phenocrysts from mantle-derived magmas: an overview of techniques, advantages and complications. Chem. Geol. 183, 5–24.

Dasgupta, R., Hirschmann, M.M., 2010. The deep carbon cycle and melting in Earth's interior. Earth Planet. Sci. Lett. 298, 1–13.

Dasgupta, R., Hirschmann, M.M., Withers, A.C., 2004. Deep global cycling of carbon constrained by the solidus of anhydrous, carbonated eclogite under upper mantle conditions. Earth Planet. Sci. Lett. 227, 73–85.

Dasgupta, R., Hirschmann, M.M., Smith, N.D., 2007. Partial melting experiments of peridotite + CO_2 at 3 GPa and genesis of alkalic ocean island basalts. J. Petrol. 48 (11), 2093–2124.

Dasgupta, R., Mallik, A., Tsuno, K., Withers, A.C., Hirth, G., Hirschmann, M.M., 2013. Carbon-dioxide-rich silicate melt in the Earth's upper mantle. Nature Lett. 493 (10), 211–216.

Delaney, J.R., Muenow, D.W., Graham, D.G., 1978. Abundance and distribution of water, carbon and sulfur in the glassy rims of submarine pillow basalts. Geochim. Cosmochim. Acta 42, 581–594.

Dixon, J., Clague, D.A., Cousens, B., Monsalve, M.L., Uhl, J., 2008. Carbonatite and silicate melt metasomatism of the mantle surrounding the Hawaiian plume: evidence from volatiles, trace elements, and radiogenic isotopes in rejuvenated-stage lavas from Niihau, Hawaii. Geochem. Geophys. Geosyst. 9 (9) (34 pp.).

Dixon, J.E., 1997. Degassing of alkalic basalts. Am. Mineral. 82, 368–378.

Dixon, J.E., Clague, D.A., 2001. Volatiles in basaltic glasses from Loihi seamount, Hawaii: evidence for a relatively dry plume component. J. Petrol. 42 (3), 627–654.

Dixon, J.E., Clague, D.A., Stolper, E.M., 1991. Degassing history of water, sulfur, and carbon in submarine lavas from Kilauea volcano, Hawaii. J. Geol. 99, 371–394.

Dixon, J.E., Stolper, E.M., Holloway, J.R., 1995. An experimental study of water and carbon dioxide solubilities in mid-ocean ridge basaltic liquids. Part I: calibration and solubility models. J. Petrol. 36, 1607–1631.

Dixon, J.E., Clague, D.A., Wallace, P., Poreda, R.R., 1997. Volatiles in alkalic basalts from the North Arch Volcanic field, Hawaii: extensive degassing of deep submarine-erupted alkalic series lavas. J. Petrol. 38 (7), 911–939.

Edgar, A.D., 1987. The genesis of alkaline magmas with emphasis on their source regions: inferences from experimental studies. In: Fitton, J.G., Upton, B.G.J. (Eds.), Alkaline Igneous Rocks. Geological Society Special Publication No. 30, pp. 29–52.

Eggler, D.H., 1978. The effect of CO_2 upon partial melting of peridotite in the system Na_2O-CaO-Al_2O_3-MgO-SiO_2-CO_2 to 35 kb, with an analysis of melting in a Peridotite-H_2O-CO_2 system. Am. J. Sci. 278, 305–343.

Esposito, R., Bodnar, R.J., Danyushevsky, L.V., de Vivo, B., Fedele, L., Hunter, J., Lima, A., Shimizu, N., 2011. Volatile evolution of magma associated with the Solchiaro eruption in the Phlegrean Volcanic District (Italy). J. Petrol. 52 (12), 2431–2460.

Esposito, R., Lamadrid, H.M., Redi, D., Steele-MacInnis, M., Bodnar, R.J., Manning, C.E., De Vivo, B., Cannatelli, C., Lima, A., 2016. Detection of liquid H2O in vapor bubbles in reheated melt inclusions: implications for magmatic fluid composition and volatile budgets of magmas? Am. Mineral. 101, 1691–1695.

Ford, C.E., Russell, D.G., Craven, J.A., Fisk, M.R., 1983. Olivine-liquid equilibria; temperature, pressure and composition dependence of the crystal/liquid cation partition coefficients for Mg, Fe2+, Ca and Mn. J. Petrol. 24, 256–265.

French, S.W., Romanowicz, B., 2015. Broad plumes rooted at the base of the Earth's mantle beneath major hotspots. Nature Lett. 525, 95–99.

Frey, F.A., Wise, W.S., Garcia, M.O., West, H., Kwon, S.-T., Kennedy, A., 1990. Evolution of Mauna Kea volcano, Hawaii: petrologic and geochemical constraints on postshield volcanism. J. Geophys. Res. 95 (B2), 1270–1300.

Frey, F.A., Clague, D., Mahoney, J.J., Sinton, J.M., 2000. Volcanism at the edge of the Hawaiian plume: petrogenesis of submarine alkalic lavas from the North Arch volcanic field. J. Petrol. 41 (5), 667–691.

Garcia, M.O., Swinnard, L., Weis, D., Greene, A.R., Tagami, T., Sano, H., Gandy, C.E., 2010. Petrology, geochemistry and geochronology of Kaua'i Lavas over 4.5 Myr: implications for the origin of rejuvenated volcanism and the evolution of the Hawaiian plume. J. Petrol. 51 (7), 1507–1540.

Gualda, G.A.R., Ghiorso, M.S., Lemons, R.V., Carley, T.L., 2012. Rhyolite-MELTS: a modified calibration of MELTS optimized for silica-rich, fluid-bearing magmatic systems. J. Petrol. 53, 875–890.

Hammer, J., Jacob, S., Welsch, B., Hellebrand, E., Sinton, J., 2016. Clinopyroxene in postshield Haleakala ankaramite: 1. Efficacy of thermobarometry. Contrib. Mineral. Petrol. 171 (7), 1–23.

Hartley, M.E., Maclennan, J., Edmonds, M., Thordarson, T., 2014. Reconstructing the deep CO2 degassing behavior of large basaltic fissure eruptions. Earth Planet. Sci. Lett. 393, 120–121.

Hauri, E.H., 1996. Major element variability in the Hawaiian mantle plume. Nature 382, 415–419.

Hauri, E.H., Maclennan, J., McKenzie, D., Gronvold, K., Oskarsson, N., Shimizu, N., 2018. CO_2 content beneath northern Iceland and the variability of mantle carbon. Geology 46 (1), 55–58.

Hémond, C., Devey, C.W., Chauvel, C., 1994. Source compositions and melting processes in the Society and Austral plumes (South Pacific Ocean): element and isotope (Sr, Nd, Pb, Th) geochemistry. Chem. Geol. 115, 7–45.

Herzberg, C., Asimow, P.D., 2008. PRIMELT3 MEGA.XLSM software for primary magma calculation: Peridotite primary magma MgO contents from the liquidus to the solidus. Geochem. Geophys. Geosyst. 16, 563–578.

Herzberg, C., Gazel, E., 2009. Petrological evidence for secular cooling in mantle plumes. Nature 458, 619–622.

Hofmann, A.H., Farnetani, C.G., 2013. Two views of Hawaiian plume structure. Geochem. Geophys. Geosyst. 14 (12), 5308–5322.
Hofmann, A.W., 2003. Sampling mantle heterogeneity through oceanic basalts: isotopes and trace elements. In: Carlson, Richard W., Holland, Heinrich D., Turekian, Karl K. (Eds.), Treatise on Geochemistry. vol. 2, pp. 61–101.
Hofmann, A.W., Jochum, K.P., 1996. Source characteristics derived from very incompatible trace elements in Mauna Loa and Mauna Kea basalts, Hawaii Scientific Drilling Project. J. Geophys. Res. 101 (B5), 11831–11839.
Hofmann, A.W., White, W.M., 1982. Mantle plumes from ancient oceanic crust. Earth Planet. Sci. Lett. 57, 421–436.
Hofmann, A.W., Feigenson, M.D., Raczek, I., 1984. Case studies in the origin of basalt. III. Petrogenesis of the Mauna Ulu eruption, Kilauea, 1969–1971. Contrib. Mineral. Petrol. 88, 24–35.
Iacono-Marziano, G., Morizet, Y., Le Trong, E., Gaillard, F., 2012. New experimental data and semi-empirical parameterization of H_2O–CO_2 solubility in mafic melts. Geochim. Cosmochim. Acta 97, 1–23.
Ito, G., Mahoney, J.J., 2005. Flow and melting of a heterogeneous mantle:2. Implications for a chemically nonlayered mantle. Earth Planet. Sci. Lett. 230, 47–63.
Johnson, D.M., Hooper, P.R., Conrey, R.M., 1999. XRF analysis of rocks and minerals for major and trace elements on a single low dilution li-tetraborate fused bead. Adv. X-ray Anal. 41, 843–867.
Jones, T.D., Davies, D.R., Campbell, I.H., Iaffaldano, G., Yaxley, G., Kramer, S.C., Wilson, C.R., 2017. The concurrent emergence and causes of double volcanic hotspot tracks on the Pacific plate. Nature 545, 472–476.
Lamadrid, H.M., Moore, L.R., Moncada, D., Rimstidt, J.D., Burruss, R.C., Bodnar, R.J., 2017. Reassessment of the Raman CO_2 densimeter. Chem. Geol. 450, 210–222.
Lange, R.A., Carmichael, I.S.E., 1990. Thermodynamic properties of silicate liquids with emphasis on density, thermal expansion, and compressibility. Rev. Mineral. 24, 25–59.
Lee, C.-T.A., Luffi, P., Plank, T., Dalton, H., Leeman, W.P., 2009. Constraints on the depths and temperatures of basaltic magma generation on Earthand other terrestrial planets using new thermobarometers for mafic magmas. Earth Planet. Sci. Lett. 279, 20–33.
Liu, M., Chase, C.G., 1991. Evolution of Hawaiian basalts: a hotspot melting model. Earth Planet. Sci. Lett. 104, 151–165.
Lloyd, A.S., Plank, T., Ruprecht, P., Hauri, E.H., Rose, W., 2013. Volatile loss from melt inclusions in pyroclasts of differing sizes. Contrib. Mineral. Petrol. 165 (1), 129–153.
Longpre, M.-A., Stix, J., Klügel, A., Shimizu, N., 2017. Mantle to surface degassing of carbon- and Sulphur-rich alkaline magma at El Hierro, Canary Islands. Earth Planet. Sci. Lett. 460, 268–280.
Maclennan, J., 2017. Bubble formation and decrepitation control the CO_2 content of olivine-hosted melt inclusions. Geochem. Geophys. Geosyst. 18 (2), 597–616.
Metrich, N., Wallace, P.J., 2008. Volatile abundances in basaltic magmas and their degassing paths tracked by melt inclusions. Rev. Mineral. Geochem. 69, 363–402.
Michael, P., 1995. Regionally distinctive sources of depleted MORB: evidence from trace elements and H_2O. Earth Planet. Sci. Lett. 131, 301–320.
Moore, J.G., 1965. Petrology of deep sea basalt near Hawaii. Am. J. Sci. 263, 40–52.
Moore, J.G., 1970. Pillow lava in a historic lava flow from Hualalai Volcano, Hawaii. J. Geol. 78 (2), 239–243.
Moore, L.R., Gazel, E., Tuohy, R., Lloyd, A.S., Esposito, R., Steele-MacInnis, M., Hauri, E.H., Wallace, P.J., Plank, T., Bodnar, R.J., 2015. Bubbles matter: an assessment of the contribution of vapor bubbles to melt inclusion volatile budgets. Am. Mineral. 100, 806–823.
Moore, L.R., Mironov, N., Portnyagin, M., Gazel, E., Bodnar, R.J., 2018. Volatile contents of primitive bubble-bearing melt inclusions from Klyuchevskoy volcano, Kamchatka: comparison of volatile contents determined by mass-balance versus experimental homogenization. J. Volcanol. Geotherm. Res. 358, 124–131.
Moussallam, Y., Edmonds, M., Scaillet, B., Peters, N., Gennaro, E., Sides, I., Oppenheimer, C., 2016. The impact of degassing on the oxidation state of basaltic magmas: a case study of Kilauea volcano. Earth Planet. Sci. Lett. 450, 317–325.
Peterson, D.W., Moore, R.B., 1987. Geologic history and evolution of geologic concepts, island of Hawaii. US Geol. Surv. Prof. Pap. 1350, 149–189.
Phillips, E.H., Sims, K.W.W., Sherrod, D.R., Salters, V.J.M., Blusztajn, J., Dulai, H., 2016. Isotopic constraints on the genesis and evolution of basanitic lavas at Haleakala, Island of Maui, Hawaii. Geochim. Cosmochim. Acta 195, 201–225.
Ren, Z.-Y., Takahashi, E., Orihashi, Y., Johnson, K.T.M., 2004. Petrogenesis of tholeiitic lavas from the Submarine Hana Ridge, Haleakala Volcano, Hawaii. J. Petrol. 45 (10), 2067–2099.
Ribe, N.M., Christensen, U.R., 1999. The dynamical origin of Hawaiian volcanism. Earth Planet. Sci. Lett. 171, 517–531.
Roedder, E., 1979. Origin and significance of magmatic inclusions. Bull. Mineral. 102, 467–510.
Rosenthal, A., Hauri, E.H., Hirschmann, M.M., 2015. Experimental determination of C, F, and H partitioning between mantle minerals and carbonated basalt, CO_2/Ba and CO_2/Nb systematics of partial melting, and the CO_2 contents of basaltic source regions. Earth Planet. Sci. Lett. 412, 77–87.
Saal, A.E., Hauri, E.H., Langmuir, C., Perfit, M.R., 2002. Vapour undersaturation in primitivemid-ocean-ridge basalt and thevolatile content of Earth's upper mantle. Nature 419, 451–455.
Sherrod, D.R., Nishimitsu, Y., Tagami, T., 2003. New K-Ar ages and the geologic evidence against rejuvenated-stage volcanism at Haleakala, East Maui, a postshield-stage volcano of the Hawaiian island chain. GSA Bull. 115 (6), 683–694.
Sherrod, D.R., Sinton, J.M., Watkins, S.E., Brunt, K.M., 2007. Geologic Map of the State of Hawai'i. US Geological Survey Open-File Report. http://pubs.usgs.gov/of/2007/1089/.
Shimizu, K., Shimizu, N., Komiya, T., Suzuki, K., Maruyama, S., Tatsumi, Y., 2009. CO_2-rich komatiitic melt inclusions in Cr-spinels within beach sand from Gorgona Island, Colombia. Earth Planet. Sci. Lett. 288, 33–43.
Shimizu, K., Saal, A.E., Myers, C.E., Nagle, A.N., Hauri, E.H., Forsyth, D.W., Kamenetsky, V.S., Niu, Y., 2016. Two-component mantle melting-mixing model for the generation of mid-ocean ridge basalts: implications for the volatile content of the Pacific upper mantle. Geochim. Cosmochim. Acta 176, 44–80.
Sides, I.R., Edmonds, M., Maclennan, J., Swanson, D.A., Houghton, B.F., 2014. Eruption style at Kilauea Volcano in Hawai'i linked to primary melt composition. Nat. Geosci. 7, 464–469.
Sobolev, A.V., Hofmann, A.W., Sobolev, S.V., Nikogosian, I.K., 2005. An olivine-free mantle source of Hawaiian shield basalts. Nature 434, 590–597.
Sobolev, A.V., Hofmann, A.W., Jochum, K.P., Kuzman, K.V., Stoll, B., 2011. A young source for the Hawaiian plume. Nature 476, 434–437.
Steele-MacInnis, M., Esposito, R., Bodnar, R.J., 2011. Thermodynamic model for the effect of post-entrapment crystallization on the H_2O-CO_2 systematics of volatile-saturated silicate melt inclusions. J. Petrol. 52, 2461–2482.
Sterner, S.M., Hall, D.L., Keppler, H., 1995. Compositional re-equilibration of fluid inclusions in quartz. Contrib. Mineral. Petrol. 119, 1–15.
Tatsumoto, M., 1978. Isotopic composition of lead in oceanic basalt and its implication to mantle evolution. Earth Planet. Sci. Lett. 38 (1), 63–87.
Tucker, J.M., Hauri, E.H., Pietruszka, A.J., Garcia, M.O., Marske, J.P., Trusdell, F.A., 2019. A high carbon content of the Hawaiian mantle from olivine-hosted melt inclusions. Geochim. Cosmochim. Acta 254, 156–172.
Wagner, T.P., Clague, D.A., Hauri, E.H., Grove, T.L., 1998. Trace element abundances of high-MgO glasses from Kilauea, Mauna Loa and Haleakala volcanoes, Hawaii. Contrib. Mineral. Petrol. 131, 13–21.
Wallace, P.J., Anderson, A.T., 1998. Effects of eruption and lava drainback on the H_2O contents of basaltic magmas at Kilauea Volcano. Bull. Volcanol. 59, 327–344.
Wallace, P.J., Kamanetsky, V.S., Cervantes, P., 2015. Melt inclusion CO_2 contents, pressures of olivine crystallization, and the problem of shrinkage bubbles. Am. Mineral. 100, 787–794.
Wanless, V.D., Shaw, A.M., 2012. Lower crustal crystallization and melt evolution atmid-ocean ridges. Nat. Geosci. 5, 651–655.
Xu, G., Frey, F.A., Clague, D.A., Weis, D., Beeson, M.H., 2005. East Molokai and other Kea-trend volcanoes: magmatic processes and sources as they migrate away from the Hawaiian hot spot. Geochem. Geophys. Geosyst. 6 (5), 1–28.